Assembly of High-Valent Oxomanganese Clusters in Aqueous Solution. Redox Equilibrium of Water-Stable $Mn_3O_4^{4+}$ and $Mn_2O_2^{3+}$ Complexes

Joseph E. Sarneski,† H. Holden Thorp,* Gary W. Brudvig, Robert H. Crabtree, and Gayle K. Schulte

Contribution from the Department of Chemistry, Yale University, New Haven, Connecticut 06511-8118. *Received March 26, 1990*

Abstract: The aqueous chemistry of a binuclear mixed-valence cluster, $[(bpy)_2Mn(O)_2Mn(bpy)_2](ClO_4)_3$ (**1**), has been investigated. The cluster exists in a pH-dependent equilibrium with a higher valent trinuclear species, $[Mn_3O_4(bpy)_4(OH_2)_2]^{4+}$ (**2**). The trinuclear cluster is favored at low pH, conditions that favor disproportionation of **1**. Evaporation of a pH 1.9 solution of **1** leads to the precipitation of red crystals of **2** in the space group $P\bar{1}$ with a = 14.902 (5) Å, b = 15.787 (5) Å, c = 12.676 (4) Å, α = 100.22 (2)°, β = 93.45 (3)°, and γ = 73.98 (3)°. A total of 3718 unique data with $I \geq 3(\sigma)I$ were refined to values of R and R_w of 8.3 and 11.3%, respectively. The temperature-dependent magnetic susceptibility shows strong antiferromagnetic coupling with ($\mathcal{H} = J(S_1 \cdot S_2) + J'(S_1 \cdot S_3 + S_2 \cdot S_3)$) g = 1.97, J = 182, cm^{-1}, and J' = 98 cm^{-1}. The $S = {}^1/_2$ ground state gives a 35-line EPR spectrum with (from simulation) g = 1.965, A_3 = 0.0066 cm^{-1}, and A_{12} = 0.0061 cm^{-1}. Electrochemistry and EPR show that the concentrations of **1** and **2** are governed by a pH-dependent equilibrium. At pH 2.5, **2** is the only species present in solution; at pH 6.5 only **1** is observable. Further, electrochemical reduction of **2** leads to the formation of **1** in aqueous solution and also in CH_3CN. The relevance of this quantitative equilibrium to the photoactivated assembly of the manganese tetramer in photosystem II is discussed.

The oxidation of water to dioxygen in higher plants is catalyzed by the enzyme photosystem II (PS II), whose active site contains a tetrameric manganese cluster (Mn_4).[1] The exact structure of Mn_4 is unknown; however, recent advances toward learning the structure have come from the synthesis of model complexes whose physical properties model those of the natural system.[2-5] Recent biochemical efforts in our laboratory have elucidated the primary events in the assembly of Mn_4; this oxidative process requires light and is termed photoactivation.[6] We report here efforts to use coordination compounds to model the assembly of the high-valent Mn cluster that occurs during photoactivation and, hence, to gain additional understanding of the structure and function of Mn_4.

In PS II, photoactivation occurs via binding and oxidation of aqueous $[Mn(OH_2)_6]^{2+}$ by the enzyme.[6] After two oxidation reactions, a stable tetramer (believed to be the S_{-1} state of Mn_4) is formed. The fundamental properties of this process are the following: (1) The oxidation of manganese leads to an increase in cluster nuclearity. (2) Because the cluster is formed from hexaaquo metal ions originally present in the bulk solution, photoactivation must occur in an environment that possesses a significant aqueous character under the conditions of cluster assembly. (3) Because water is the substrate of the catalytic reaction, the cluster must also be accessible to the aqueous environment during the S-state cycle.

Our initial efforts in the area of functional modeling have involved characterizing the thermodynamics of proton-coupled electron transfer in a mixed-valence dimer, $[(bpy)_2Mn(O)_2Mn(bpy)_2]^{3+}$ (**1**),[7] which has been studied extensively as a model for the manganese cluster.[8] Weighardt et al.[9] have studied the proton-dependent disproportionation of Mn^{III}_2 complexes, showing that protonation of a bridging oxo ligand can lead to redox chemistry. We are interested in proton-coupled electron transfer because we have previously proposed that water oxidation involves steps in which deprotonation of aquo and hydroxo ligands is coupled to oxidation of manganese;[2-5,10] similar proposals have been made regarding other oxo-bridged metalloenzymes.[11] This work has led us to an understanding of the conditions under which high-valent manganese is stable in aqueous solution and has elucidated an aqueous chemistry of high-valent manganese that is unexpected on the basis of other known systems.

In modeling the fundamental processes of photoactivation in PS II, we have studied the interconversion of the $[Mn^{III,IV}_2O_2]^{3+}$ dimer (**1**) and a trinuclear $[Mn^{IV}_3O_4]^{4+}$ species, $[Mn_3O_4(bpy)_4(OH_2)_2]^{4+}$ (**2**). Both of these complexes are stable in aqueous solution, and we will show evidence here that, under certain conditions, these two complexes are the only forms of manganese present in solution. The amounts of **1** and **2** present in solution are governed by a pH-dependent equilibrium that is quantitatively reversible and does not lead to the production of physiologically incompatible manganese products such as MnO_2.

A complex that is analogous to **2**, $[Mn^{IV}_3O_4(bpy)_4Cl_2]^{2+}$, has been synthesized and structurally characterized.[12] In this synthesis, the $[Mn_3O_4]^{4+}$ core was prepared in nonaqueous (DMF) solution by use of de novo synthesis from Mn^{2+} and MnO_4^-. The complex is structurally analogous to **2** and its magnetic properties are similar, but the formation of $[Mn_3O_4(bpy)_4Cl_2]^{4+}$ in nonaqueous solution would not lead one to predict that **2** could be the elusive oxidation and/or protonation product of **1** that is present in aqueous solution.

Experimental Methods

$[Mn_3O_4(bpy)_4(OH_2)_2]^{4+}$, X-ray quality, red-brown crystals having the formula $[Mn_3O_4(bpy)_4(OH_2)_2](ClO_4)_4 \cdot 5H_2O$ were obtained by slow (1-week) evaporation of a pH 1.9 (HNO_3) solution containing 30 mg of dimer **1** (prepared as in ref 8). It was these crystals for which the complete structure reported here was determined; however, because of the small scale of the reaction, the yield was difficult to determine. The following procedure can be used reproducibly to prepare the trinuclear species **2** in a slightly different crystal form.

In an attempt to prepare larger quantities of **2**, 2.0 g of **1** was added to 700 mL of water and acidified (HNO_3) to pH 1.9. Slow evaporation at ambient temperature to ~25 mL yielded 1.2 g of lustrous black

† On leave from the Department of Chemistry, Fairfield University, Fairfield, CT 06430.

(1) Brudvig, G. W.; Beck, W. F.; dePaula, J. C. *Annu. Rev. Biophys. Biophys. Chem.* **1989**, *18*, 25.
(2) Brudvig, G. W.; Crabtree, R. H. *Prog. Inorg. Chem.* **1989**, *37*, 99.
(3) Vincent, J. B.; Christou, G. *Adv. Inorg. Chem.* **1989**, *33*, 197.
(4) Weighardt, K. *Angew. Chem., Int. Ed. Engl.* **1989**, *28*, 1153.
(5) Pecoraro, V. L. *Photochem. Photobiol.* **1988**, *48*, 249.
(6) (a) Tamura, N.; Cheniae, G. M. *FEBS Lett.* **1986**, *200*, 231. (b) Miller, A.-F.; Brudvig, G. W. *Biochemistry* **1989**, *28*, 8181.
(7) Thorp, H. H.; Sarneski, J. E.; Brudvig, G. W.; Crabtree, R. H. *J. Am. Chem. Soc.* **1989**, *111*, 9249.
(8) (a) Cooper, S. R.; Calvin, M. *J. Am. Chem. Soc.* **1977**, *99*, 6623. (b) Cooper, S. R.; Dismukes, G. C.; Klein, M. P.; Calvin, M. *J. Am. Chem. Soc.* **1978**, *100*, 5248.
(9) Weighardt, K.; Bossek, U.; Nuber, B.; Weiss, J.; Bonvoisin, J.; Corbella, M.; Vitols, S. E.; Girerd, J.-J. *J. Am. Chem. Soc.* **1988**, *110*, 7398.
(10) Brudvig, G. W.; Crabtree, R. H. *Proc. Natl. Acad. Sci. U.S.A.* **1986**, *83*, 4586.
(11) Lippard, S. J. *Angew. Chem., Int. Ed. Engl.* **1988**, *27*, 344.
(12) Auger, N.; Girerd, J.-J.; Corbella, M.; Gleizes, A.; Zimmerman, J.-L. *J. Am. Chem. Soc.* **1990**, *112*, 448.

0002-7863/90/1512-7255$02.50/0

Table I. Crystallographic Data for **2**.

emp form	$C_{40}H_{33}O_{25}N_8Cl_4Mn_3$
M_r	1332.36
cryst syst	triclinic
space gp	$P\bar{1}$ (No. 2)
temp, °C	25
a, Å (25 reflcns)	14.902 (5)
b, Å	15.787 (5)
c, Å	12.676 (4)
α, deg	100.22 (2)
β, deg	93.45 (3)
γ, deg	73.98 (3)
V, Å^3	2821 (3)
Z	2
cryst dimens, mm	0.80 × 0.50 × 0.08
cryst dens, calcd, g/cm^3	1.569
radiation, Mo Kα, Å	0.71069
abs coeff, cm^{-1}	9.09
$2\theta_{max}$, deg	50.0
total no. of data	9853
no. of obsd data [$I \geq 3\sigma(I)$]	3718
no. of refinement param	634
$R = \sum\|\|F_o\| - \|F_c\|\|/\|F_o\|$	0.083
$R_w = [\sum_w(\|F_o\| - \|F_c\|)^2/\sum wF_o^2]^{1/2}$	0.113
goodness of fit	3.04

crystals of $[Mn_3O_4(bpy)_4(OH_2)_2](ClO_4)_4 \cdot {}^1/_2[bpyH_2(NO_3)_2] \cdot 2H_2O$ (yield 90%, based on eq 1). Anal. Calcd for $C_{45}H_{45}N_{10}O_{27}Cl_4Mn_3$: C, 36.91; H, 3.10; N, 9.56; Cl, 9.68; Mn, 11.25. Found: C, 36.81; H, 3.45; N, 9.38; Cl, 9.72; Mn, 11.29. X-ray crystallographic data for this crystal form show it to be triclinic, space group $P\bar{1}$ (No. 2),[13a] a = 14.696 (5) Å, b = 17.472 (5) Å, c = 12.560 (4) Å, α = 108.47 (2)°, β = 93.88 (3)°, γ = 82.97 (3)°, and Z = 2. The crystal density was determined to be 1.616 g/cm^3 by flotation in CCl_4 and tetrachloroethane; the calculated crystal density is 1.60 g/cm^3. Iodometric analysis[13b] shows the gram equivalent weight to be 235 ± 10, in good agreement with 244 calculated from the molecular formula. X-ray data show the manganese cluster to be identical in both crystal forms.

Measurements. Cyclic voltammetry,[7] EPR spectroscopy,[13c] and Clark electrode analysis[13d] were performed at Yale as described previously. All electrochemical potentials are versus SSCE. Magnetic susceptibility data were taken on finely powdered samples at the Francis Bitter National Magnet Laboratory at MIT with an SHE SQUID magnetometer. The data were corrected for sample diamagnetism.[14] X-ray photoelectron spectroscopy (XPS) was done at the University of North Carolina—Chapel Hill on an instrument that has been described.[15]

X-ray Crystallography. All X-ray data were collected on an Enraf-Nonius CAD4 diffractometer with graphite-monochromated Mo Kα radiation. Further details are given in Table I.

Results and Discussion

Synthesis of $[Mn_3O_4]^{4+}$. The instability of **1** at low pH has been observed previously.[8a] This chemistry had been assigned to protonation of an oxo bridge possibly followed by hydrolysis to monomeric products; a pK_a of 2.3 was determined by both optical spectroscopy and solution magnetic susceptibility. In attempting to elucidate the precise molecular events in this process, we noticed that evaporation of an aqueous solution of $[(bpy)_2Mn(O)_2Mn(bpy)_2](ClO_4)_3$ (**1**) acidified with HNO_3 (pH 1.9) leads to precipitation of red-brown crystals having the formula $[Mn_3(O)_4(bpy)_4(OH_2)_2](ClO_4)_4 \cdot 5H_2O$ (**2**).

The net reaction in the synthesis of **2** is shown in eq 1. We have observed both Mn^{2+} and **2** by EPR and can quantitatively account for all of the manganese redox equivalents in eq 1. While

$$\underset{\mathbf{1}}{2Mn^{III,IV}{}_2(O)_2(bpy)_4{}^{3+}} + 4H^+ \rightarrow \underset{\mathbf{2}}{Mn^{IV}{}_3(O)_4(bpy)_4(OH_2)_2{}^{4+}} + Mn^{2+} + 4bpyH^+ \quad (1)$$

Table II. Selected Bond Distances (Å) and Angles (deg) for **2**

a. Bonds

Mn(1)–O(2)	1.79 (1)	Mn(1)–O(1)	1.80 (1)
Mn(1)–O(4)	1.83 (1)	Mn(1)–O(5)	2.04 (1)
Mn(1)–N(2)	2.04 (1)	Mn(1)–N(1)	2.05 (1)
Mn(2)–O(2)	1.81 (1)	Mn(2)–O(1)	1.82 (1)
Mn(2)–O(3)	1.85 (1)	Mn(2)–O(6)	2.05 (1)
Mn(2)–N(3)	2.04 (1)	Mn(2)–N(4)	2.06 (1)
Mn(3)–O(3)	1.76 (1)	Mn(3)–O(4)	1.77 (1)
Mn(3)–N(8)	1.99 (1)	Mn(3)–N(5)	2.01 (1)
Mn(3)–N(6)	2.07 (1)	Mn(3)–N(7)	2.09 (1)

b. Angles

O(2)–Mn(1)–O(1)	83.5 (5)	O(2)–Mn(1)–O(4)	98.0 (5)
O(2)–Mn(1)–O(5)	175.5 (5)	O(2)–Mn(1)–N(2)	89.5 (5)
O(2)–Mn(1)–N(1)	90.1 (5)	O(1)–Mn(1)–O(5)	95.7 (5)
O(1)–Mn(1)–O(4)	96.1 (5)	O(2)–Mn(1)–Mn(2)	42.2 (3)
O(1)–Mn(1)–N(2)	93.6 (5)	O(1)–Mn(1)–N(1)	169.9 (5)
O(1)–Mn(1)–Mn(2)	42.6 (4)	O(4)–Mn(1)–O(5)	86.4 (5)
O(4)–Mn(1)–N(2)	168.3 (5)	O(4)–Mn(1)–N(1)	92.6 (5)
O(4)–Mn(1)–Mn(2)	91.2 (4)	O(5)–Mn(1)–N(2)	86.1 (5)
O(5)–Mn(1)–N(1)	90.1 (5)	O(5)–Mn(1)–Mn(2)	137.8 (3)
N(2)–Mn(1)–N(1)	78.4 (5)	N(2)–Mn(1)–Mn(2)	100.4 (4)
N(1)–Mn(1)–Mn(2)	132.1 (4)	O(2)–Mn(2)–O(1)	82.4 (5)
O(2)–Mn(2)–O(3)	95.3 (5)	O(2)–Mn(2)–N(3)	93.5 (5)
O(2)–Mn(2)–O(6)	96.7 (5)	O(2)–Mn(2)–N(4)	166.3 (5)
O(2)–Mn(2)–Mn(1)	41.7 (3)	O(1)–Mn(2)–O(3)	96.9 (5)
O(1)–Mn(2)–N(3)	93.8 (5)	O(1)–Mn(2)–O(6)	177.2 (5)
O(1)–Mn(2)–N(4)	87.1 (5)	O(1)–Mn(2)–Mn(1)	42.0 (3)
O(3)–Mn(2)–N(3)	167.0 (5)	O(3)–Mn(2)–O(6)	85.8 (5)
O(3)–Mn(2)–N(4)	94.7 (5)	O(3)–Mn(2)–Mn(1)	90.0 (3)
N(3)–Mn(2)–O(6)	83.6 (5)	N(3)–Mn(2)–N(4)	78.3 (6)
N(3)–Mn(2)–Mn(1)	103.0 (4)	O(6)–Mn(2)–N(4)	93.3 (5)
O(6)–Mn(2)–Mn(1)	137.7 (4)	N(4)–Mn(2)–Mn(1)	129.0 (4)
O(3)–Mn(3)–O(4)	100.7 (5)	O(3)–Mn(3)–N(8)	97.4 (6)
O(3)–Mn(3)–N(5)	91.7 (5)	O(3)–Mn(3)–N(6)	84.8 (5)
O(3)–Mn(3)–N(7)	169.1 (6)	O(4)–Mn(3)–N(8)	89.7 (5)
O(4)–Mn(3)–N(5)	95.2 (5)	O(4)–Mn(3)–N(6)	172.1 (6)
O(4)–Mn(3)–N(7)	89.4 (5)	N(8)–Mn(3)–N(5)	168.6 (5)
N(8)–Mn(3)–N(6)	95.1 (6)	N(8)–Mn(3)–N(7)	78.5 (6)
N(5)–Mn(3)–N(6)	78.9 (6)	N(5)–Mn(3)–N(7)	91.3 (6)
N(6)–Mn(3)–N(7)	85.5 (5)		

the overall mechanism must be quite complex, the formation of **2** in this medium can be understood in terms of the initial disproportionation reaction (eq 2). From our measurements on the

$$2Mn^{III,IV}{}_2(O)_2(bpy)_4{}^{3+} + H^+ \rightarrow Mn^{III}{}_2(O)(OH)(bpy)_4{}^{3+} + Mn^{IV}{}_2(O)_2(bpy)_4{}^{4+} \quad (2)$$

energetics of proton-coupled electron transfer in this system,[7] the K_{eq} for eq 2 increases by 5 orders of magnitude when the pH is lowered from 7 to 2.5; we have also established from the pH dependence of the III,IV/III,III redox couple that the III,III product is protonated. In the initial studies,[7] the pH was kept sufficiently high to avoid formation of **2**. At low pH, the disproportionation reaction occurs, and subsequent chemistry involving loss of bpy and core rearrangement leads to the formation of **2**. From the known chemistry of these complexes,[2-5] it would be expected that the $Mn^{III}{}_2$ complex is the most labile towards bpy loss. Indeed, isolation of bis(μ-oxo)dimanganese(III) dimers has been elusive except in one case where a sterically encumbering ligand was used to stabilize this oxidation state.[16] In contrast, many analogous $Mn^{IV}{}_2$ dimers have been structurally characterized.[17]

An ORTEP projection of **2** is shown in Figure 1. Crystallographic data and bond distances and angles are given in Tables I and II; the somewhat high (8.3%) value for R is a result of disorder in the ClO_4^- counterions. The complex contains a (μ-$O)_2Mn_2$ unit bridged by an additional O–Mn–O linkage. The Mn(1)···Mn(2) separation of 2.679 Å is characteristic of a (μ-$O)_2Mn_2$ group. The other Mn···Mn separations, where the only bridging ligands are single μ_2-oxo groups, are 3.246 and 3.263 Å. Recent EXAFS results on PS II show two Mn···Mn separations

(13) (a) *International Tables for Crystallography*; Kynoch Press: Birmingham, England, 1974; Vol. IV. (b) Kulawiec, R. J. Ph.D. Thesis, Yale University, 1989. (c) Beck, W. F.; Innes, J. B.; Lynch, J. B.; Brudvig, G. W. *J. Magn. Reson.*, in press. (d) Beck, W. F.; dePaula, J. C.; Brudvig, G. W. *Biochemistry* **1985**, *24*, 3035.

(14) O'Connor, C. J. *Prog. Inorg. Chem.* **1982**, *29*, 203.

(15) Cabaniss, G. E.; Diamantis, A. A.; Murphy, W. R., Jr.; Linton, R. W.; Meyer, T. J. *J. Am. Chem. Soc.* **1985**, *107*, 1845.

(16) Goodson, P. A.; Hodgson, D. J. *Inorg. Chem.* **1989**, *28*, 3606.

(17) Christou, G. *Acc. Chem. Res.* **1989**, *22*, 328.

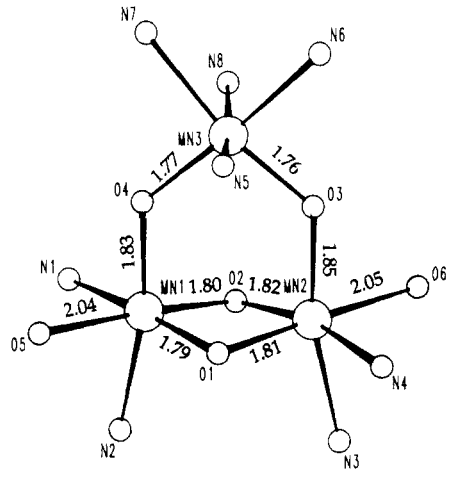

Figure 1. Core structure of **2**, showing anisotropic thermal parameters, atom-labeling scheme, and Mn–O bond distances (Å).

of 2.7 and 3.3 Å.[18] Like a number of other oxomanganese clusters,[2-5,12,17] our two unique distances are in good agreement with those seen in the natural system. Further, the structural parameters of our complex and the Cl^- analogue[12] are similar; specific comparisons will be discussed below.

An unusual feature of **2** is that, for the first time, water is found in the coordination sphere of Mn^{IV}; the state of protonation is clear from the long (2.04 Å) Mn–OH_2 bond lengths. The metal centers containing the aquo moieties are ligated to one bpy and *three* bridging oxo groups. Thus, this ligand set is sufficiently strongly donating to stabilize an unusually high-valent metal center to the extent that coordinating water remains fully protonated. This is, no doubt, a result of the strongly donating nature of the bridging oxo ligands and the low pH at which **2** is stable. In addition, our complex and the Cl^- analogue[12] contain two chemically inequivalent pairs of oxo bridges, a feature not yet seen in oxomanganese clusters of nuclearities <6.[17]

The crystallographic characterization of **2** clarifies a number of points concerning the aqueous chemistry of **1**. In two reports, **2** was present under conditions similar to ours; however, the structure was not correctly assigned. Cooper and Calvin, in their original report of the acid–base chemistry of **1**,[8a] presented optical spectra as a function of pH. Their pH 0.5 spectrum is identical with that of an authentic sample of **2** at low pH or in nonaqueous solution. Additionally, Khangulov et al.[19] have reported the EPR spectrum of a species obtained from the chemical oxidation of **1** in aqueous solution. The complex has been assigned as the one-electron oxidation product, $[Mn^{IV}_2O_2(bpy)_4]^{4+}$; however, the EPR spectrum is identical with that of **2**, discussed below.

Physical Properties of 2. The temperature dependence of the magnetic moment (μ_{eff}) of **2** is shown in Figure 2 from 4.6 to 300 K. The magnetic moment increases from 1.71 μ_B at 4.6 K to 3.77 μ_B at 292 K, indicative of strong antiferromagnetic coupling between metal centers.

The general spin Hamiltonian was simplified by assuming Mn(1) and Mn(2) to be equivalent, giving a coupling scheme as shown in the inset of Figure 2. Thus, the two distinct coupling parameters represent the interaction across the di-μ-oxo bridge (J) and across the mono-μ-oxo bridges (J'). The resulting spin Hamiltonian is given in eq 3. The eigenvalues of this Hamiltonian

$$\mathcal{H} = J(S_1 \cdot S_2) + J'(S_1 \cdot S_3 + S_2 \cdot S_3) \qquad (3)$$

can be determined by using the Kambe vector coupling method[20] as in eq 4. The energies of the system are therefore given by eq

$$S_{12} = S_1 + S_2 \qquad S = S_{12} + S_3 \qquad (4)$$

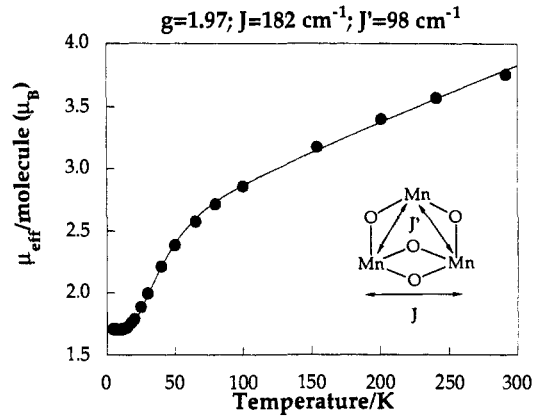

Figure 2. Temperature dependence of the magnetic moment of **2**. The solid line is a least-squares fit to the data with the indicated parameters; see text.

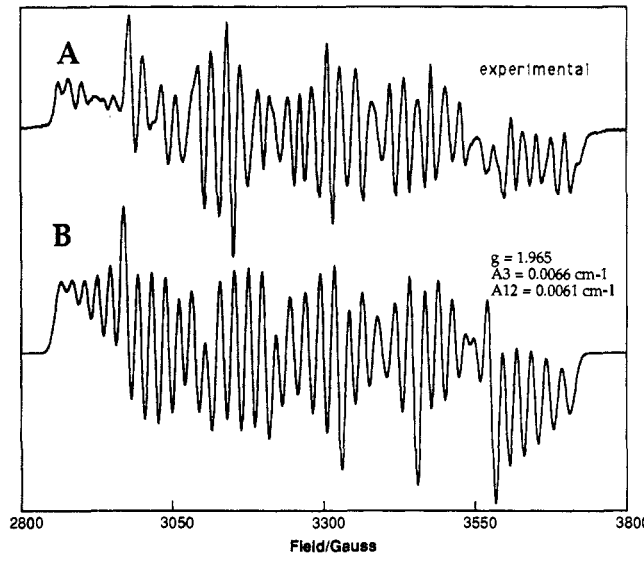

Figure 3. (A) X-band EPR spectrum of **2** (1 mM) in a 30% ethylene glycol glass at 9 K: microwave frequency, 9.05 GHz; modulation frequency, 100 kHz; modulation amplitude, 2 G; microwave power, 5 μW. (B) Simulated EPR spectrum: g = 1.965, A_3 = 0.0066 cm^{-1}, A_{12} = 0.0061 cm^{-1}, line width = 11 G.

5. For the nine unpaired electrons, there are 12 individual spin levels.

$$E = (J/2)[S_{12}(S_{12} + 1) - 15/2] + (J'/2)[S(S + 1) - S_{12}(S_{12} + 1) - S_3(S_3 + 1)] \qquad (5)$$

With the Van Vleck equation and the spin-only formula,[21] an expression was derived for μ_{eff} as a function of temperature. A least-squares fit of the data gives g = 1.97, J = 182 cm^{-1}, and J' = 98 cm^{-1}.[22] Calculation of the energies of the spin state of **2** shows that the ground state has a total spin $S = {}^1/_2$ (S_{12} = 1) with an $S = {}^3/_2$ (S_{12} = 0) excited state at 63 cm^{-1}. This is of interest since thermally adjacent $S = {}^1/_2$ and $S = {}^3/_2$ states have been invoked to explain how the EPR signals of the S_2 state of PS II could come from the same cluster.[1,23,24]

(18) (a) George, G. N.; Prince, R. C.; Cramer, S. P. *Science* **1989**, *243*, 789. (b) Penner-Hahn, J. E.; Fronko, R. M.; Pecoraro, V. L.; Yocum, C. F.; Betts, S. D.; Bowlby, N. R. *J. Am. Chem. Soc.* **1990**, *112*, 2549.

(19) Khangulov, S. V.; Goldfeld, M. G.; Kirpichnikova, N. P.; Dobryakov, S. N.; Ilyasova, V. B. *J. Chem. Soc., Chem. Commun.* **1989**, 1755.

(20) Kambe, K. *J. Phys. Soc Jpn.* **1950**, *5*, 48.

(21) Van Vleck, J. H. *Theory of Electric and Magnetic Susceptibilities*; Oxford University Press: London, 1932.

(22) The complete equation used for fitting the susceptibility data is given in the supplementary material.

(23) Li, X.; Kessissoglou, D. P.; Kirk, M. L.; Bender, C. J.; Pecoraro, V. L. *Inorg. Chem.* **1988**, *27*, 1.

(24) Brudvig, G. W. In *Advanced EPR*; Hoff, A. J., Ed.; Elsevier: New York, 1989, p 839.

Our calculated exchange coupling parameters are similar to those of Girerd et al.;[12] however, we observe a somewhat larger J and a somewhat smaller J'. This can be ascribed to the larger trans effect of Cl^- versus H_2O, which leads to a contraction of the (Mn1, Mn2)–(O1, O2) bonds in the aquo complex, facilitating the electronic communication between Mn1 and Mn2. To accommodate this structural perturbation, the other Mn–ligand distances increase. A decrease or increase in the bond lengths would be expected to lead to a corresponding increase or decrease, respectively, in the antiferromagnetic coupling, and this is observed.

Since the ground state of the cluster has $S = {}^1/_2$, it is expected to give a $g = 2$ EPR signal.[24] For a trinuclear Mn species (I(Mn) $= {}^5/_2$), a multiline signal would be expected. For solutions of **2** in glassing solvents, a 35-line pattern in the $g = 2$ region is observed (Figure 3A). The spectrum was simulated by taking advantage of the results of the magnetic susceptibility study, which showed that Mn(1) and Mn(2) can be considered equivalent at the level of the magnetic properties of the complex. The simulation was then performed by treating the complex as a dimer of Mn(3) ($I_3 = {}^5/_2$, $S_3 = {}^3/_2$) coupled to the Mn(1)–Mn(2) pair ($I_{12} = 5$, $S_{12} = 1$); the spin states were known from the susceptibility fit. Two isotropic Mn hyperfine coupling constants were used: A_3 gave a 6-line pattern coming from the Mn(3), and A_{12} split each of the 6 lines into an 11-line pattern coming from the Mn(1)–Mn(2) pair. The intensities of the 11-line pattern were corrected to account for the overlapping of lines from two metal centers, the resulting pattern had intensities of 1:2:3:4:5:6:5:4:3:2:1. A good simulation (Figure 3B) was obtained with the following isotropic parameters: $g = 1.965$, $A_3 = 0.0066$ cm^{-1}, $A_{12} = 0.0061$ cm^{-1}, and line width = 11 G. It is noteworthy that the spectrum of **2**, which contains 35 lines and an average splitting between lines of ~23 G, is significantly different from the S_2-state multiline signal of PS II, which contains approximately 20 lines with an average splitting of 87.5 G; an alternate proposal has been advanced that a trinuclear Mn cluster is the paramagnetic species giving rise to the S_2-state multiline signal.[5]

Spectra similar to that shown in Figure 3A have been simulated on two other occasions. Girerd et al. successfully simulated the spectrum of the chloro analogue using a more elaborate model.[12] In their simulation, the g value and the hyperfine coupling were treated anisotropically, each taken to have axial symmetry; further, the two chemically equivalent manganese ions were made inequivalent. With these considerations, the total number of simulation parameters comes to nine. We have achieved an equally good simulation using only four parameters and a completely isotropic system, pointing to the fact that the approximations made in fitting the magnetic susceptibility data are also valid in simulating the EPR spectrum. This is of interest because we have proposed that the multiline signal of PS II can be simulated with a model using vector coupling of two Mn···Mn pairs.[24] In the second reported simulation of the 35-line spectrum,[19] it was assumed incorrectly that the EPR-active species was a weakly coupled Mn(IV)–Mn(IV) dimer. The simulation does not adequately reproduce the gross features of the spectrum. This is no doubt due to the improper assignment of the structure of the EPR-active species.

In addition to magnetic properties, an understanding of the X-ray spectroscopy of manganese complexes is also desirable for the assignment of the oxidation state of Mn_4 from X-ray absorption spectroscopy K edges measured for the natural system.[25] We have measured the X-ray photoelectron spectra (XPS) for **1** and **2** to understand how the overall electron density at the manganese centers changes in the interconversion of the two complexes. The charge-corrected binding energies for **1** are 642.2 eV ($2p_{3/2}$) and 653.7 eV ($2p_{1/2}$); the corresponding values for **2** are 642.6 and 654.1 eV. The 0.4 eV increase in energy is indicative of an increase in oxidation state of the metal and is reasonable for a net change in oxidation state of $Mn^{3.5+} \rightarrow Mn^{4+}$. The

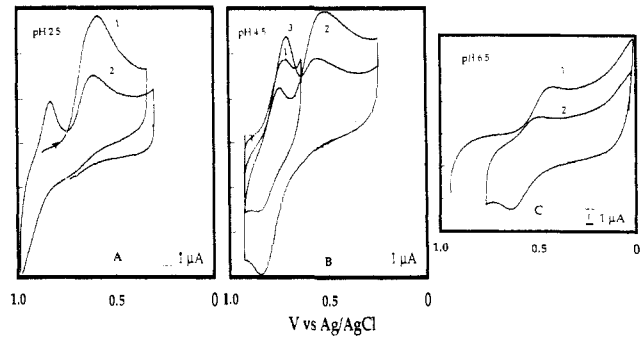

Figure 4. Cyclic voltammograms of **2** in phosphate buffer (0.1 M) at (A) pH 2.5, (B) pH 4.5, and (C) pH 6.5: working electrode, activated glassy carbon; auxiliary electrode, Pt wire; reference electrode, SSCE; scan rate, 50 mV/s.

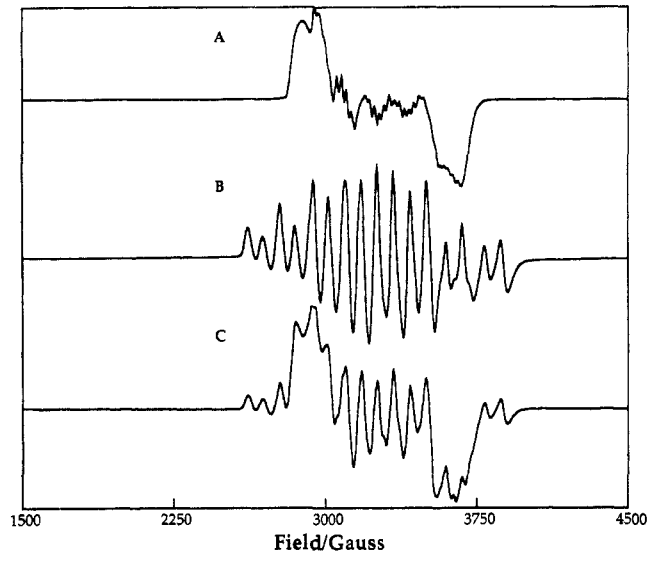

Figure 5. EPR spectra of (A) **2** in 0.5 M HNO_3; (B) **1** in CH_3CN; (C) **2** in 0.05 M bpy buffer, pH 4.5. Concentrations of complexes were 1 mM; other conditions are as in Figure 3A.

standard manganese reference compound, $[Mn^{III}(CN)_6]^{3-}$, has binding energies of 641 and 652 eV.[26] A complete set of XPS data for high-valent oxomanganese clusters has been obtained, and these data will be the subject of a separate publication.[27]

Solution Chemistry: Cyclic Voltammetry. The nonaqueous electrochemistry of **1** is characterized by two redox couples corresponding to reversible IV,IV/III,IV and irreversible III,-IV/III,III reductions.[8a] The potential of these couples is strongly dependent on the nature of the ancillary ligands.[28] For the bpy complex (**1**) these potentials are $E_{1/2}$(IV,IV/III,IV) = 1.2 V and E_p(III,IV/III,III) = 0.25 V (SSCE). The cyclic voltammogram of **2** in CH_3CN shows an irreversible reduction at 0.36 V. Upon scanning through this reduction, waves corresponding to a reversible oxidation at 1.15 V and an irreversible reduction at 0.25 V appear. These couples are indicative of the III,IV dimer **1**[8a] and appear only after scanning through the reduction wave for **2**. Thus, it appears from the nonaqueous electrochemistry that reduction of trimer **2** leads to formation of dimer **1**. Since the synthesis of **2** occurs via lowering the pH of an aqueous solution of **1** (and we have established in our earlier work that low pH leads

(25) Guiles, R. D.; Zimmerman, J. L.; McDermott, A. E.; Yachandra, V. K.; Cole, J. L.; Dexheimer, S. L.; Britt, R. D.; Weighardt, K.; Bossek, U.; Sauer, K.; Klein, M. P. *Biochemistry* **1990**, *29*, 471.

(26) Siegbahn, K.; Nordling, C.; Fahlmer, A.; Nordberg, R.; Hamrin, K.; Hedman, J.; Johannson, G.; Bergmark, T.; Karlsson, S.-E.; Lindgren, I.; Lindberg, B. *ESCA: Atomic, Molecular and Solid State Structure Studied by Means of Electron Spectroscopy*; Royal Society of Sciences: Uppsala, Sweden, 1967.

(27) Thorp, H. H.; Kulawiec, R. J.; Sarneski, J. E.; Papaefthymiou, G.; Brudvig, G. W.; Crabtree, R. H. Submitted for publication.

(28) Goodson, P. A.; Glerup, J.; Hodgson, D. J.; Michelsen, K.; Pedersen, E. *Inorg. Chem.* **1990**, *29*, 503.

to conditions that encourage oxidation of **1**),[7] compounds **1** and **2** are the thermodynamic sinks under reducing and oxidizing conditions, respectively.

In the aqueous electrochemistry, the relationship between pH and redox potential is strikingly evident. At pH 2.5 (Figure 4A), the cyclic voltammogram of **2** shows that on scan 1 there is no dimer present and the only observable redox couple is the irreversible reduction of **2** at ~0.6 V. After reducing **2**, however, dimer **1** is detectable on scan 2 at 0.9 V (the anodic component is obscured by the solvent background). This wave is attributable to proton-coupled reduction of **2**; accordingly, the potential is shifted positively relative to nonaqueous solution.[7] At pH 4.5 (Figure 4B), **1** is present on the first scan at 0.75 V. On scan 2, the reduction wave for **2** is evident at 0.5 V, and upon scanning through the dimer region again (scan 3), it is clear that more of **1** has been produced. A concomitant decrease in current for **2** is observed. Finally, at pH 6.5 (Figure 4C), only the dimer is present at 0.56 V. Adjusting the pH of this solution in the 2.5–6.5 range allows the voltammograms in Figure 4A, B to be reproduced. The pH dependence of the irreversible redox couple for **2** makes it is clear that this reduction is proton-coupled (1 e^-/1 H^+).[29] Likewise, the proton-coupled nature of the dimer electrochemistry is also evident, as has been established previously.[7]

Solution Chemistry: EPR. The electrochemistry results suggest that **2** is stable at low pH but is in equilibrium with **1** at pH 4.5. Since both of these complexes have characteristic EPR signals, this should be straightforward to confirm. As discussed above, trimer **2** gives a 35-line spectrum in glassing solvents and mixtures (Figure 3A); however, in nonglassing solvents such as pure water or acetonitrile, a broad signal is seen in the same region. The loss of hyperfine structure is no doubt due to intermolecular spin–spin interactions in aggregates induced by freezing in nonglassing solvents. In fact, the line width of the signal appears to be inversely proportional to the quality of the glass formed.

Our electrochemical results indicate that at low pH the trimer is stable as the only form of manganese in solution. Indeed, the EPR spectrum of **2** in 0.5 M HNO_3 (Figure 5A) shows the characteristic spectrum of **2** with some loss of hyperfine structure due to the lack of formation of a glass upon freezing. Our pH 4.5 electrochemical results indicate that at this pH a mixture of **1** and **2** is present. The spectrum taken at pH 4.5 (Figure 5C) is clearly that of a mixture of **1** (Figure 5A) and **2** (Figure 5B). Quantitation of manganese present in the solution by integration of the EPR spectrum shows that all of the manganese is observed in this measurement. Under these conditions, **1** and **2** are stable and do not decompose to such species as Mn^{2+} or MnO_2.

The conversion of **1** to **2** proceeds via a mechanism different from the conversion of **2** to **1**. In the acidification of **1**, we have established by quantitative EPR that Mn^{2+} is generated, according to eq 1. We have performed experiments in which solutions of **1**, which have been acidified to form **2** + Mn^{2+}, are treated with base to give **1** in quantitative yield. This solution can be acidified to give **2** + Mn^{2+}, again in quantitative yield. Thus, the equilibrium is completely reversible with essentially complete recovery of the complex.

In the conversion of **1** to **2**, all of the redox equivalents are accounted for. The reverse reaction, when induced by raising the pH of an aqueous solution of **2**, is distinct in two ways. First, the reaction occurs on a slower time scale of several hours as opposed to instantaneously. Second, **2** is converted quantitatively to **1** as determined by EPR. Hence, a non-manganese species must supply the reducing equivalent needed for the conversion of **2** to **1**. We have established unambiguously from Clark electrode measurements that water is not being oxidized to dioxygen. The formation of H_2O_2 can also be ruled out because **1** and its analogues are efficient catalysts for the dismutation of H_2O_2 to H_2O and O_2,[30] which would have been detected by Clark electrode analysis. Thus, the most likely fate of the extra oxidizing equivalent is an organic conversion, such as the oxidation of bipyridine to bipyridine *N*-oxide.

Scheme I

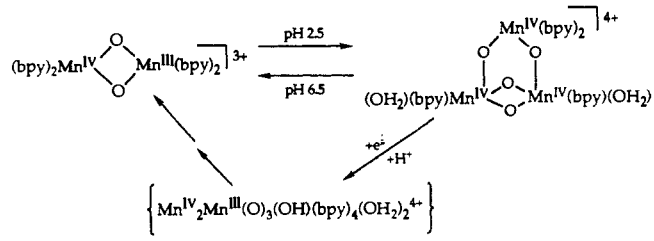

The chemistry that is apparent from our EPR and electrochemical measurements is summarized in Scheme I. As can be inferred from our earlier work on proton-coupled electron transfer in **1**,[7] conditions of low pH are overall oxidizing toward the complex. At sufficiently low pH, the equilibrium favors **2** according to eq 1; however, the reverse reaction proceeds without the production of manganese products other than **1**. The conversion of **2** to **1** can also be effected by electrochemical reduction. The pH dependence of the electrochemistry indicates that the intermediate is the product of a one-electron, one-proton reduction as shown. Rush and Maskos[30] have obtained kinetic evidence for a similar trinuclear III,IV,IV intermediate in the dismutation of H_2O_2 by $[Mn_2O_2(edda)_2]^-$ (edda = ethylenediamine-*N*,*N*′-diacetate).

Conclusions

The existence of **2** in aqueous solutions of **1** has escaped proper assignment on two occasions. Some years ago, Cooper and Calvin reported the pH-dependent optical spectroscopy of **1**, assigning the spectral changes to protonation of the oxo bridge.[8a] We have measured the optical spectrum of **2** and find that it is identical with the low-pH spectrum reported by these workers. In addition, Khangulov and co-workers recently reported a 35-line, $g = 2$ EPR spectrum obtained after the oxidation of **1** in aqueous solution.[19] The spectrum was assigned to a $[Mn^{IV}_2(O)_2(bpy)_4]^{4+}$ dimer in which the two metal centers are weakly coupled. The reported spectrum, however, is identical with the EPR spectrum of **2** obtained in 30% ethylene glycol (Figure 3A).

In aqueous solution, **1** and **2** are in equilibrium; this is noteworthy for a number of reasons.

First, the observation in aqueous solution of an increase in nuclearity coupled to an overall oxidation of the cluster models the fundamental properties of the photoactivation process of PS II described above. This process occurs without precipitation of insoluble, physiologically incompatible products such as MnO_2.

Second, the stable equilibrium between **1** and **2** is a revealing observation with regard to the chemistry of high-valent manganese in the natural system. Our results show that conditions do exist where assembly of high-valent clusters can proceed in aqueous solution without production of undesirable manganese products such as Mn^{2+} or MnO_2. Previous ideas regarding the aqueous chemistry of high-valent manganese held that only tightly bound ligands would stabilize these clusters in aqueous solution.[31] This notion would lead to high-valent clusters that are unreactive and coordinatively inert in water; such is the case of the adamantane cluster $[Mn_4O_6(TACN)_4]^{4+}$ (TACN = 1,4,7-triazacyclononane).[4] In contrast, we find that coordinatively labile high-valent manganese clusters not only can be stable in water but can undergo the reversible rearrangements reported here. The oxidized cluster **2** is also quite stable toward water at low pH, as emphasized by the presence of two unprecedented Mn^{IV}–aqua moieties seen in the crystal structure. Thus, by regulating effective pH and potential in the thylakoid membrane, the natural system may promote smooth, oxidative assembly of Mn_4 by chemistry analogous to that reported here.

(29) Bard, A. J.; Faulkner, L. R. *Electrochemical Methods*; Wiley: New York, 1980.

(30) Rush, J. D.; Maskos, Z. *Inorg. Chem.* **1990**, *29*, 897.

(31) Cotton, F. A.; Wilkinson, G. *Advanced Inorganic Chemistry*, 5th ed.; Wiley: New York, 1988.

Acknowledgment. We thank Dr. Jeffrey R. Bocarsly for helpful discussions. We thank Dr. G. Papaefthymiou for help with the SQUID measurements. We thank the National Institutes of Health for support of this research through Grants GM-32715 and GM-40974 and the NSF for support (J.E.S.).

Supplementary Material Available: Tables listing temperature dependence, positional parameters, intramolecular distances and bond angles, torsion or conformation angles, and U values (19 pages); observed and calculated structure factors (26 pages). Ordering information is given on any current masthead page.

Spin Pairing and Magnetic Coupling in Quasi One-Dimensional Semiconductors with a Trimeric Stacking Structure. Structural, Charge-Transport, and Magnetic Studies of $[Ni(tatbp)]_3[ReO_4]_2 \cdot C_{10}H_7Cl$ and $[Cu(tatbp)]_3[ReO_4]_2 \cdot C_{10}H_7Cl$

Martin R. Godfrey, Timothy P. Newcomb, Brian M. Hoffman,* and James A. Ibers*

Contribution from the Department of Chemistry and Materials Research Center, Northwestern University, Evanston, Illinois 60208. *Received January 8, 1990*

Abstract: Electrochemical oxidation of (triazatetrabenzoporphyrinato)nickel(II) or (triazatetrabenzoporphyrinato)copper(II), Ni(tatbp) or Cu(tatbp), dissolved in 1-chloronaphthalene in the presence of the perrhenate ion affords the new molecular conductors $[Ni(tatbp)]_3[ReO_4]_2 \cdot C_{10}H_7Cl$ and $[Cu(tatbp)]_3[ReO_4]_2 \cdot C_{10}H_7Cl$. The isostructural compounds are composed of partially ligand-oxidized (+2/3) M(tatbp) molecules that form trimerized stacks. Trimerization of the conducting stacks renders the compounds semiconductors with conductivity along the needle axis (crystallographic a) in the range of 2.5×10^{-4}–3.0×10^{-4} Ω^{-1} cm^{-1} and an activation energy for conduction in the range of 0.24–0.26 eV. Magnetic susceptibility measurements on the Ni(II) derivative show that the valence band has the diamagnetic ground state expected for a semiconductor. Nonetheless, the valence-band electrons are shown to mediate a strong intratrimer Cu–Cu coupling characterized by a Weiss constant $\theta = -5.2$ K in the Cu(II) analogue. The magnetic properties are rationalized in terms of a band structure derived by considering the trimers as weakly interacting supermolecules, with θ dominated by intratrimer interactions. A structure determination was performed on the Cu(II) analogue. It crystallizes in space group C_i^1–$P\bar{1}$ of the triclinic system with one formula unit in a cell of dimensions $a = 9.167$ (6) Å, $b = 15.849$ (10) Å, $c = 16.065$ (10) Å, $\alpha = 65.87$ (2)°, $\beta = 72.11$ (3)°, and $\gamma = 84.01$ (2)° (volume = 2126 Å^3) at 110 K. The Cu–Cu distance for adjacent macrocycles within a trimer is 3.190 (3) Å and that between trimers is 3.482 (4) Å. The ReO_4^- anions lie within channels formed between the stacks as does a disordered 1-chloronaphthalene solvent molecule. The final refinement of 4988 observations having $F_o^2 > 3\sigma(F_o^2)$ involved an anisotropic model for Cu and Re, an isotropic model for the other non-hydrogen atoms, and fixed positions for the hydrogen atoms (295 variables). The refinement converged to values of $R(F) = 0.085$ and $R_w(F) = 0.091$.

Introduction

We have described a series of molecular conductors prepared by chemical oxidation of metalloporphyrins with molecular iodine.[1-7] These compounds are comprised of metal-over-metal stacks of partially oxidized (+1/3) metallomacrocycles (M(L)) surrounded by chains of I_3^- anions.[8,9] When oxidation occurs from the ligand-based p-π orbitals the result often is a highly conductive molecular metal. For example, crystals of Ni(pc)I (pc = phthalocyaninato), Cu(pc)I, and Cu(tatbp)I (tatbp = triazatetrabenzoporphyrinato) have room temperature conductivities of up to 750 Ω^{-1} cm^{-1} and Ni(pc)I has been shown to retain a metallic band structure even at very low temperatures.[1]

In the compounds Cu(pc)I and Cu(tatbp)I the carrier electrons in the ligand-based p-π conduction band interact with the magnetic

(1) (a) Schramm, C. J.; Scaringe, R. P.; Stojakovic, D. R.; Hoffman, B. M.; Ibers, J. A. *J. Am. Chem. Soc.* **1980**, *102*, 6702–6713. (b) Martinsen, J.; Greene, R. L.; Palmer, S. M.; Hoffman, B. M.; Ibers, J. A. *J. Am. Chem. Soc.* **1983**, *105*, 677–678. (c) Martinsen, J.; Palmer, S. M.; Tanaka, J.; Greene, R. L.; Hoffman, B. M. *Phys. Rev. B* **1984**, *30*, 6269–6276.

(2) Martinsen, J.; Pace, L. J.; Phillips, T. E.; Hoffman, B. M.; Ibers, J. A. *J. Am. Chem. Soc.* **1982**, *104*, 83–91.

(3) Pace, L. J.; Martinsen, J.; Ulman, A.; Hoffman, B. M.; Ibers, J. A. *J. Am. Chem. Soc.* **1983**, *105*, 2612–2620.

(4) Martinsen, J.; Stanton, J. L.; Greene, R. L.; Tanaka, J.; Hoffman, B. M.; Ibers, J. A. *J. Am. Chem. Soc.* **1985**, *107*, 6915–6920.

(5) Hoffman, B. M.; Ibers, J. A. *Acc. Chem. Res.* **1983**, *16*, 15–21.

(6) (a) Ogawa, M. Y.; Martinsen, J.; Palmer, S. M.; Stanton, J. L.; Tanaka, J.; Greene, R. L.; Hoffman, B. M.; Ibers, J. A. *J. Am. Chem. Soc.* **1987**, *109*, 1115–1121. (b) Ogawa, M. Y.; Hoffman, B. M.; Lee, S.; Yadkowsky, M.; Halperin, W. P. *Phys. Rev. Lett.* **1986**, *57*, 1177–1180.

(7) (a) Liou, K. K.; Ogawa, M. Y.; Newcomb, T. P.; Quirion, G.; Lee, M.; Poirier, M.; Halperin, W. P.; Hoffman, B. M.; Ibers, J. A. *Inorg. Chem.* **1989**, *28*, 3889–3896. (b) Quirion, G.; Poirier, M.; Ogawa, M. Y.; Hoffman, B. M. *Solid State Commun.* **1987**, *64*, 613–616. (c) Quirion, G.; Poirier, M.; Liou, K. K.; Ogawa, M. Y.; Hoffman, B. M. *Phys. Rev. B* **1988**, *37*, 4272–4275. (d) Ogawa, M. Y.; Palmer, S. M.; Liou, K. K.; Quirion, G.; Thompson, J. A.; Poirier, M.; Hoffman, B. M. *Phys. Rev. B* **1989**, *39*, 10682–10692.

(8) Similar structures are produced by electrochemical oxidation of metallomacrocycles. (a) Yakushi, K.; Yamakado, H.; Yoshitake, M.; Kosugi, N.; Kuroda, H.; Sugano, T.; Kinoshita, M.; Kawamoto, A.; Tanaka, J. *Bull. Chem. Soc. Jpn.* **1989**, *69*, 687–696. (b) Yakushi, K.; Yamakado, H.; Yoshitake, M.; Kosugi, N.; Kuroda, H.; Kowamoto, A.; Tanaka, J.; Sugano, T.; Kinoshita, M.; Hino, S. *Synth. Met.*, **1989**, *29*, F95–F102. (c) Almeida, M.; Kanatzidis, M. G.; Tonge, L. M.; Marks, T. J.; Marcy, H. O.; McCarthy, W. J.; Kannewurf, C. R. *Solid State Commun.* **1987**, *63*, 457–461. (d) Newcomb, T. P.; Godfrey, M. R.; Hoffman, B. M.; Ibers, J. A. *J. Am. Chem. Soc.* **1989**, *111*, 7078–7084.

(9) Other structural types have been prepared with M(pc) systems of higher coordination number. For example see: (a) Wynne, K. J. *Inorg. Chem.* **1985**, *24*, 1339–1343. (b) Hanack, M. *Mol. Cryst. Liq. Cryst.* **1988**, *160*, 133–137. (c) Mossoyan-Deneux, M.; Benlian, D.; Baldy, A.; Pierrot, M. *Mol. Cryst. Liq. Cryst.* **1988**, *156*, 247–256. (d) Mossoyan-Deneux, M.; Benlian, D.; Pierrot, M.; Fournel, A.; Sobier, J. P. *Inorg. Chem.* **1985**, *24*, 1878–1882. (e) Pietro, W. J.; Marks, T. J.; Ratner, M. A. *J. Am. Chem. Soc.* **1985**, *107*, 5387–5391.

0002-7863/90/1512-7260$02.50/0